Simulation of pupil-plane observation of angle-of-arrival fluctuations in daytime turbulence

A. Berdja[a], A. Irbah[a], J. Borgnino[b] and F. Martin[b]

[a]CRAAG - Observatoire d'Alger, BP 63 Bouzaréah, Algiers, Algeria
[b]Univ. Nice-Sophia Antipolis, UMR 6525 - Parc Valrose, F-06108 Nice Cedex 2, France

ABSTRACT

High angular resolution observations of the sun are limited by atmospheric turbulence. The MISOLFA seeing monitor (still under construction) is developed to obtain spatial and temporal statistical properties of optical turbulence by analyzing local motions observed on solar edge images. The solar Flying Shadows used for Angle-of-Arrival spatio-temporal analysis are observed in the pupil-plane image by mean of a rectangular thin slit positioned on the solar edge image. A numerical simulation of the light propagation in both the atmospheric turbulence medium and the MISOLFA optical system is carried out studying the relation of the measured intensity variations in the pupil-plane to Angle-of-Arrival fluctuations in the non-isoplanatic case. First results are presented and discussed.

Keywords: Site testing, Atmospheric turbulence, Remote sensing

1. INTRODUCTION

Observations of the Sun at High Angular Resolution using ground-based telescopes need an accurate modelling of the optical effects induced by atmospheric turbulence. To illustrate the problem, we consider the case of solar diameter measurements. Since more than 25 years, diameter measurements are performed at Calern Observatory (Observatoire de la Côte d'Azur) with the solar astrolabe showing inexplicable apparent variations.[1] More recently, a new experiment (DORaySol)[3] has been implemented on the same site for the same objectives. Soon (2007-2008), a spatial experiment (PICARD (CNES)) will be launched to perform solar diameter and solar irradiance measurements in Space.[2] SODISM II, a replica of one of PICARD instruments, will be installed near the two present operational experiments of the Calern site to allow simultaneous measurements. The main objectives are the comparison of the results deduced firstly from spatial data and secondly from ground data, as well as the evaluation of atmospheric turbulence optical effects on measurements performed from the ground.The ground observations will thus, be qualified using space data and appropriate inverse techniques.

A seeing monitor must allow the modelling of these effects. It must give, in the framework of a turbulent model (Von Kàrmàn's model, for example), the values of the integrated optical parameters (Fried's parameter r_0, spatial coherence outer scale $\mathcal{L}_0$, size of isoplanatic patch θ_0, correlation time for the fluctuations τ_0), but also the vertical profile of the optical turbulence energy given by the structure constant of the air refractive index fluctuations $C_n^2(h)$. Such a generalized monitor could be used for evaluation of sites where telescopes dedicated to the Sun observations should be installed but also could equip every solar observatory. MISOLFA (*Moniteur d'Images SOLaires Franco-Algérien*) is developed for that purpose.

The MISOLFA principle is based on the statistical analysis of Angle-of-Arrival (AA) fluctuations, which are fluctuations at each point of the normal of the perturbed wave-fronts. The AA-fluctuations can directly be observed in the image plane (case of Shack-Hartmann's sensors used in adaptive optics) but also in the pupil plane if the observed astronomical sources (for example, Sun or Moon) present an intensity distribution with a strong discontinuity.

Further author information: (Send correspondence to A. Irbah)
A. Berdja : E-mail: berdja@scientist.com
A. Irbah : E-mail: irbah@aerov.jussieu.fr, Telephone: +33 (0)1 64 47 43 58, Address: Service Aéronomie, B.P. 3, 91371 Verrièrres le Buisson, France

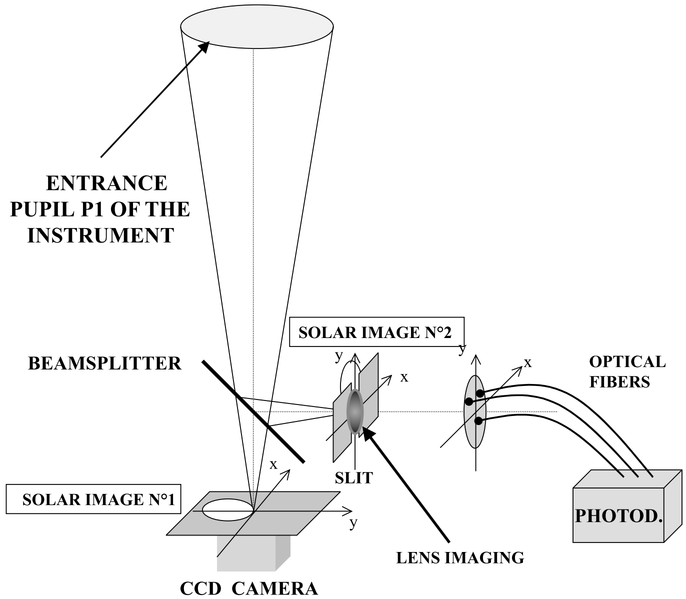

Figure 1. MISOLFA : experimental device.

The monitor experimental device is built so as to have 2 analysis ways (Fig. 1). On the first way, a CCD camera placed on the solar limb image allows to record directly the AA-fluctuations.[8] A beam splitter creates a second way, named in the following *pupil plane observation way* in which the telescope pupil is observed through a narrow slit placed on the solar limb image.

2. PUPIL-PLANE OBSERVATION WAY OF MISOLFA

Many works have been developed on image plane observations[9, 16] but few ones on the pupil-plane observations. Thus, a complete numerical simulation of this observation way is needed to better understand all filtering affecting AA-fluctuation measurements performed in the pupil-plane.

The *pupil-plane observation way* of MISOLFA consists in imaging the telescope entrance pupil with a recombining lens through a narrow diaphragm placed in the focal plane on the solar limb. The diaphragm size is some arc-seconds wide and about fifty arc-seconds length. To record pupil intensity fluctuations, several photodiodes connected via optical fibers will be put on the image behind diaphragms of different sizes. This signal given by the different photodiodes will be simultaneously recorded. A spatiotemporal analysis may be performed leading to estimate all atmospheric parameters.

Geometrical optics will be helpful to understand how the *pupil plane observation way* of MISOLFA works. Light rays of the atmospheric perturbed wave-front undergo random angles and pass or no through the diaphragm. Thus, the pupil illumination observed through the diaphragm will be related to the local slopes of the wave-front.

In case of an extended source, the good situation is that a linear relationship exists between intensity variations $I(\overrightarrow{r})$ in the pupil-plane image and AA-fluctuations $\underline{\alpha}(\overrightarrow{r})$ at the entrance pupil :

$$\underline{\alpha}(\overrightarrow{r}) \propto I(\overrightarrow{r}) \tag{1}$$

where $\propto$ denotes the proportionality operator.

Previous works have shown however, the goodness at the first order of the relationship between intensity and AA-fluctuations.[5, 6] Now, we will study the validity limits of Equation (1). We present first in the next section, the theoretical aspects used for developing the numerical simulation.

3. THEORETICAL MODEL

We need a mathematical formulation to perform the numerical simulation of the occurring process. In a first stage, we consider a monochromatic wave coming from a given point-source situated in the $\overrightarrow{\alpha_0}$ direction, where $\overrightarrow{\alpha_0}$ denotes a two-dimensional angle. The complex amplitude of such a wave at ground level may be expressed as $\sqrt{I_0(\overrightarrow{\alpha_0})}\psi_{\overrightarrow{\alpha_0}}(\overrightarrow{r})\exp(\frac{2\pi i}{\lambda}\overrightarrow{\alpha_0}\overrightarrow{r})$, where $\overrightarrow{r}$ is a space vector in the pupil-plane, λ the monochromatic wave wavelength, $I_0(\overrightarrow{\alpha_0})$ an angular distribution of the incident light intensity and $\psi_{\overrightarrow{\alpha_0}}(\overrightarrow{r})$ is the normalized turbulence-disturbed complex amplitude of the light wave.

3.1. Diffraction Through the Entrance Pupil

The propagation trough the telescope of the wave-front limited to its entrance pupil forms a Fraunhoffer diffraction pattern in the instrument focal plane. The angular distribution $K_{\overrightarrow{\alpha_0}}(\overrightarrow{\alpha})$ is then expressed by :

$$K_{\overrightarrow{\alpha_0}}(\overrightarrow{\alpha}) \propto \int d\overrightarrow{r} G_p(\overrightarrow{r})\sqrt{I_0(\overrightarrow{\alpha_0})}\psi_{\overrightarrow{\alpha_0}}(\overrightarrow{r})\exp(\frac{2\pi i}{\lambda}\overrightarrow{\alpha_0}\overrightarrow{r})\exp(\frac{-2\pi i}{\lambda}\overrightarrow{\alpha}\overrightarrow{r}) \tag{2}$$

where $\overrightarrow{\alpha}$ are two-dimensional angular coordinates. $G_p(\overrightarrow{r})$ is the so-called pupil function equal to one inside the pupil area and to zero outside.

Let us note $TF_0(f(\overrightarrow{r})) = F(\overrightarrow{\alpha})$ the Fourier transform of $f(\overrightarrow{r})$ evaluated for the reduced space frequencies $\overrightarrow{r}/\lambda$: $TF_0(f(\overrightarrow{r})) = \int d\overrightarrow{r} f(\overrightarrow{r})\exp(\frac{-2\pi i}{\lambda}\overrightarrow{\alpha}\overrightarrow{r})$. Equation 2 is then rewritten as :

$$K_{\overrightarrow{\alpha_0}}(\overrightarrow{\alpha}) \propto TF_0(G_p(\overrightarrow{r})\sqrt{I_0(\overrightarrow{\alpha_0})}\psi_{\overrightarrow{\alpha_0}}(\overrightarrow{r})\exp(\frac{2\pi i}{\lambda}\overrightarrow{\alpha_0}\overrightarrow{r})) \tag{3}$$

$K_{\overrightarrow{\alpha_0}}(\overrightarrow{\alpha})$ is a speckled angular distribution of complex amplitude and $|K_{\overrightarrow{\alpha_0}}(\overrightarrow{\alpha})|^2$ is the so-called *PSF* (Point-Spread Function) used in image formation theory. It is a speckle image of the point source as shown in the third figure of Fig. 5.

The speckled distribution $K_{\overrightarrow{\alpha_0}}(\overrightarrow{\alpha})$ is not centered on the optical axis but is in the $\overrightarrow{\alpha_0}$ incidence angle direction. Thus, it is more or less masked according to its position relatively to diaphragm borders (see the fourth figure of Fig. 5).

3.2. Pupil Image Reconstruction Over the Diaphragm

The pupil-plane image is formally obtained by operating an inverse Fourier transform on the complex amplitude $K_{\overrightarrow{\alpha_0}}(\overrightarrow{\alpha})$ over the diaphragm : $TF_0^{-1}(F(\overrightarrow{\alpha})) = \int d\overrightarrow{r} F(\overrightarrow{\alpha})\exp(\frac{2\pi i}{\lambda}\overrightarrow{\alpha}\overrightarrow{r})$. The complex amplitude $K'_{\overrightarrow{\alpha_0}}(\overrightarrow{r})$ obtained at the observation plane is then given by :

$$K'_{\overrightarrow{\alpha_0}}(\overrightarrow{r}) \propto TF_0^{-1}(G_s(\overrightarrow{\alpha})K_{\overrightarrow{\alpha_0}}(\overrightarrow{\alpha})\exp(\frac{2\pi i}{\lambda}\overrightarrow{\alpha}\overrightarrow{r})) \tag{4}$$

where $G_s(\overrightarrow{\alpha})$ is the angular transmission of the diaphragm.

In both Equations (3) and (4), we have not taken into account symmetries induced by the internal reflecting light within the telescope. However, the pupil image coordinates can easily be scaled so as to correspond to the entrance pupil ones.

Since $K_{\overrightarrow{\alpha_0}}(\overrightarrow{\alpha})$ is relatively not centered onto $G_s(\overrightarrow{\alpha})$, the partial masking will be more or less important depending directly of $\overrightarrow{r}$ and the angular distribution itself. Intensity fluctuations $I_{\overrightarrow{\alpha_0}}(\overrightarrow{r}) = |K'_{\overrightarrow{\alpha_0}}(\overrightarrow{r})|^2$ will be then observed in the pupil-plane image. They are what we are calling the *Flying Shadows* obtained for the incidence angle $\overrightarrow{\alpha_0}$.

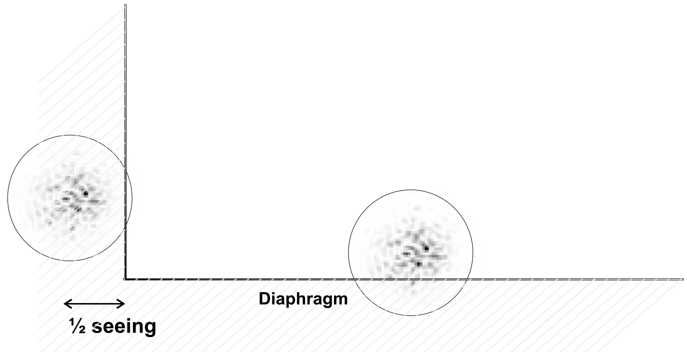

Figure 2. Two intensity distributions (*PSF*'s) partially masked by diaphragm borders. The *PSF* left-side contributes to the pupil-plane image formation unless it is situated at 1/2 seeing angle outside the diaphragm area.

3.3. The Case of an Extended Source

The resulting intensity fluctuations for an extended source in the pupil-plane image is the summation over the angular field-of-view allowed by the optical system of all source-point intensity contributions. The diaphragm angular size conjointly to the seeing angle define the angular integration domain as shown in Fig. 2.

If we express the finite angular integration domain by an angular transmission function $G_{s,seeing}(\overrightarrow{\alpha_0})$, the intensity image of the pupil-plane is then given by :

$$I(\overrightarrow{r}) \propto \int d\overrightarrow{\alpha_0} G_{s,seeing}(\overrightarrow{\alpha_0}) |TF_0^{-1}(G_s(\overrightarrow{\alpha}) \exp(\frac{2\pi i}{\lambda} \overrightarrow{\alpha} \overrightarrow{r}) TF_0(G_p(\overrightarrow{r}) \sqrt{I_0(\overrightarrow{\alpha_0})} \psi_{\overrightarrow{\alpha_0}}(\overrightarrow{r}) \exp(\frac{2\pi i}{\lambda} \overrightarrow{\alpha_0} \overrightarrow{r})))|^2 \quad (5)$$

Equation 5 is the basic mathematical model used to develop the numerical simulation presented in this work.

4. EXPECTED OPTICAL LIMITATIONS

The use of a diaphragm of a finite size in the focal plane introduces additional effects which limit AA-fluctuation analysis from intensity measurements of the pupil-plane images. Two effects were highlighted and have been studied by Borgnino and Martin.[5] They are related to the *diffraction* and *angular* filtering by the diaphragm.

4.1. Diffraction Filtering

Diffraction over the diaphragm causes a blurring on the resulting pupil-plane images due to a space-frequency filtering. This filtering is not easy to express and we will consider Equation (2) to summarize it. From this Equation, $K_{\overrightarrow{\alpha_0}}(\overrightarrow{\alpha})$ can be considered as the complex spectrum of the spatial contents of the perturbed wave-front at the entrance pupil (expressed by $\psi_{\overrightarrow{\alpha_0}}(\overrightarrow{r})$). This spectrum is randomly limited by the diaphragm area due to both the angular positions $\overrightarrow{\alpha_0}$ and the speckled pattern $K_{\overrightarrow{\alpha_0}}(\overrightarrow{\alpha})$ itself carrying out to express with difficulty the introduced filtering.

To illustrate the diffraction filtering, Fig. 3 shows a simulation of intensity patterns obtained for an extended source in case of three different diaphragm widths and unspecified seeing conditions.

Although these enumerated conceptual difficulties, it is possible to have a significant description of diffraction blurring[5] by considering some average behavior in case of an extended source. A diaphragm with an angular width w_x allows to observe in the pupil plane details with angular separation greater than about λ/Fw_x, F denoting the telescope focal length. In the entrance pupil plane, they correspond to spatial separations of about λ/w_x. Thus, the presence of the diaphragm in the focal plane is equivalent to a high spatial frequency filter with a cut-off frequency f_d given by :

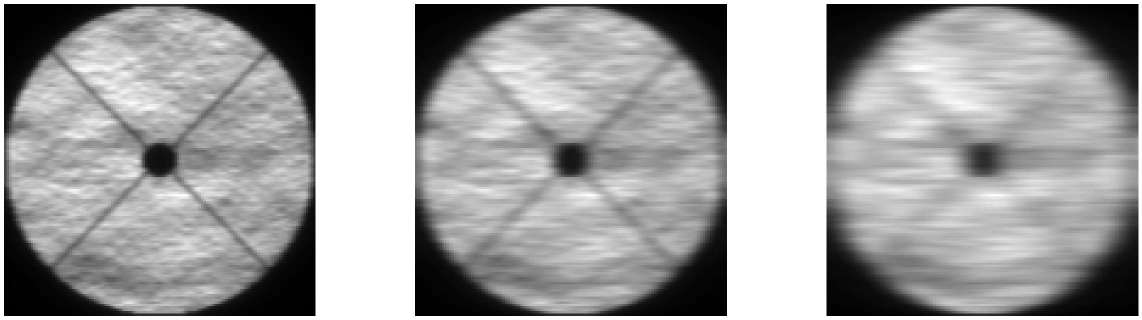

Figure 3. Simulation of Flying Shadows of an extended object of uniform luminosity (no darkening) obtained for three different diaphragm widths (see Sect.5.1). For all cases, the same optical turbulence is considered at the entrance pupil and near-field approximation is assumed. The angular width w_x of diaphragms is respectively equal from the left to the right, to $8''$, $4''$ and $2''$.

$$f_d \approx w_x/\lambda \tag{6}$$

According to this known filtering, we have to use a diaphragm as large as possible. However, increasing the diaphragm width has consequences on the angular filtering.

4.2. Angular Filtering

In case of an extended source such as the sun, the image obtained with the *pupil plane observation way* of MISOLFA is the superposition of all individual images formed by each source-point located by its angular position $\overrightarrow{\alpha_0}$ (see section 3.3). It means that the turbulence-induced perturbations are integrated over the angular field-of-view, which in our case is limited to the angular extent of the diaphragm and to the local average seeing angle (see Sect.3.3).

Anisoplanatism expresses the dependence of the optical turbulence with lines-of-sight. It is more or less important following the turbulent layer positions and angular separations of object points. Thus, the angular integration introduces an additional blurring on pupil plane images corresponding to another space frequency filtering.

Figure 4 shows image blurring effect induced by anisoplanatism in case of an extended object. It shows that blurring in the pupil plane images depends also on seeing conditions via anisoplanatism.

This anisoplanatic filtering is also not easy to express but some simple considerations lets to have a significant estimation.

Geometrical considerations allow to say that details in a turbulent layer situated at an altitude h have spatial dimensions on the pupil plane of about hw_x. As a consequence, we are not able to see on the pupil plane images, turbulence features smaller than about hw_x for the considered single turbulent layer at the altitude h. We can then define a spatial cut-off frequency f_a for the anisoplanatism angular filter as :

$$f_a \approx 1/hw_x \tag{7}$$

According to this additional filtering, we better use a diaphragm as thin as possible but in this case, the diffraction filtering increases.

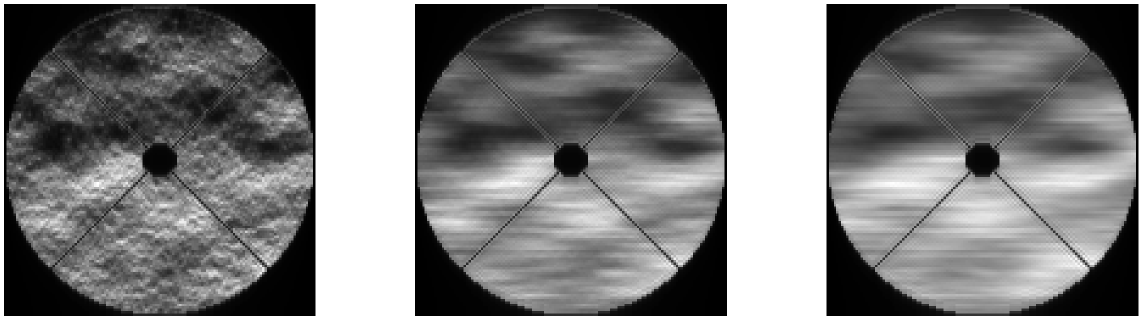

Figure 4. Simulation of Flying Shadows obtained for an extended source in both isoplanatic and anisoplanatic cases (see Sect.5.1). The object has an uniform luminosity (no darkening) and a same optical turbulence is considered at the entrance pupil. The diaphragm width w_x is equal to $5''$ for all figures. In the left figure, total isoplanatism is assumed contrarily to the others where anisoplanatism is considered along the diaphragm width. In the third one, bad seeing is also considered ($\approx 10''$). The turbulent layer properties are $h = 500m$, $r_0 = 1cm$ and $\mathcal{L}_0 = 10m$. Note that anisoplanatic filtering would be more important along the diaphragm length and will depend on the solar darkening profile.

4.3. The Choice of Diaphragm's width

The previous developments on the *diffraction* and *angular* filtering by the diaphragm show antagonist effects. In fact, for a given altitude of the turbulent layer, the optical system is mostly limited by anisoplanatism if w_x is too large and the limitation comes from diffraction if w_x is too small.

As shown by Borgnino and Martin,[5] the best practical compromise for w_x is certainly the case for which the two filtering are equivalent so that $f_a \approx f_d$ and then :

$$w_x \approx \sqrt{\lambda/h} \tag{8}$$

In case of observations performed with MISOLFA at a wavelength λ equal to $535.7nm$, a diaphragm width $w_x = 5''$ allows to remote turbulent layers lower than $h = 911m$.

4.4. Scintillation

In most of seeing monitors based on AA-fluctuation measurement analysis, scintillation is neglected and near-field approximation is assumed. In the pupil plane observation approach, scintillation cannot be ignored since we measure intensity fluctuations. Indeed, intensity measurements could be perturbed by scintillation if turbulent layers are localized at high altitudes.

However, for MISOLFA's diurnal measurements, it is expected that turbulent layers are mostly situated near the ground so that scintillation effects could be negligible.

5. NUMERICAL SIMULATION - FIRST RESULTS

5.1. Obtaining Flying Shadows by Simulation

The numerical simulation is based on the formal description of the optical device expressed by Equation 5.

First at all, we have to provide instantaneous complex amplitude $\sqrt{I_0(\overrightarrow{\alpha_0})}\psi_{\overrightarrow{\alpha_0}}(\overrightarrow{r})$ of atmospheric perturbed wave-fronts at the telescope entrance pupil. We assume that the optical effects induced by the whole turbulence may be expressed as an equivalent single turbulent layer positioned at a given altitude h above the instrument. To calculate $\psi_{\overrightarrow{\alpha_0}}(\overrightarrow{r})$ for every $\overrightarrow{\alpha_0}$, we take the part of the simulated turbulent layer corresponding to its projection over the telescope pupil following the $\overrightarrow{\alpha_0}$ direction. The perturbed wave-fronts are obtained using a modified Monte Carlo procedure refereed as Nakajima's method.[14] Optical perturbations from this method are the

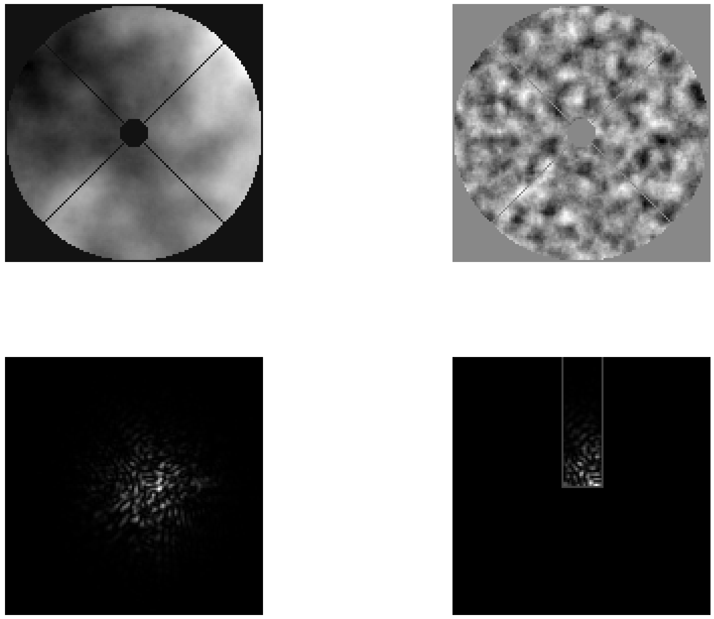

Figure 5. Figures showing some steps of simulation (see Sect.5.1) in case of a single point-source located in α_0 angular direction. They are obtained for a same optical turbulence at the entrance pupil. The figures on the top (from left to right) are phase and amplitude distributions simultaneously generated for the optical wave-front $\psi_{\alpha_0}(r)$ at the entrance pupil. The figures on the bottom represent respectively the intensity of the angular distribution $K_{\alpha_0}(\alpha)$ (PSF) (left) and the portion of $|K_{\alpha_0}(\alpha)|^2$ passing through the diaphragm placed in the focal plane.

inverse Fourier transform of a random complex quantity which statistical variance is equal to the theoretical one corresponding to the considered model (Kolmogorov, Von Kàrmàn ...).

The optical turbulence simulator we implemented gives simultaneously phase and amplitude fluctuations corresponding to the same generated turbulence sample (see Fig. 5).

A Fourier Transform is then applied to $\psi_{\overrightarrow{\alpha_0}}(\overrightarrow{r})$ limited to the telescope pupil area in order to obtain the angular distribution of the complex amplitude $K_{\overrightarrow{\alpha_0}}(\overrightarrow{\alpha})$ in the focal plane. Fig. 5 shows its intensity which corresponds also to the *PSF*. Note that the influence of $\overrightarrow{\alpha_0}$ will be taken into account after when diaphragm effects will be considered. A special attention is accorded in the simulation to the sampling path of the $K_{\overrightarrow{\alpha_0}}(\overrightarrow{\alpha})$-matrix which is wavelength dependence.

The diaphragm effects consist by keeping a randomly part of $K_{\overrightarrow{\alpha_0}}(\overrightarrow{\alpha})$ (see Fig. 5). The extracted part is linked to the relative angle $\overrightarrow{\alpha_0}$ which expresses also anisoplanatism with h in case of the equivalent impulse layer model.

The corresponding pupil-plane image related to the $\overrightarrow{\alpha_0}$ incidence direction is then obtained by applying an inverse Fourier Transform to $K_{\overrightarrow{\alpha_0}}(\overrightarrow{\alpha})$ and taking the square modulus to get the intensity $I_{\overrightarrow{\alpha_0}}(\overrightarrow{r})$.

The whole process is repeated for every incident angle $\overrightarrow{\alpha_0}$ of the angular domain allowed by the second way of MISOLFA optical system (see Sect.3.3). All $I_{\overrightarrow{\alpha_0}}(\overrightarrow{r})$ contributions are then summed over this angular domain in order to get the global image intensity $I(\overrightarrow{r})$.

5.2. Observation of AA-fluctuations in Pupil-Plane Images

AA-fluctuations are defined by the local slopes of the perturbed wave-fronts. They are formally expressed by the space-derivative of the phase fluctuations at the entrance pupil. We are then able to test the pupil plane

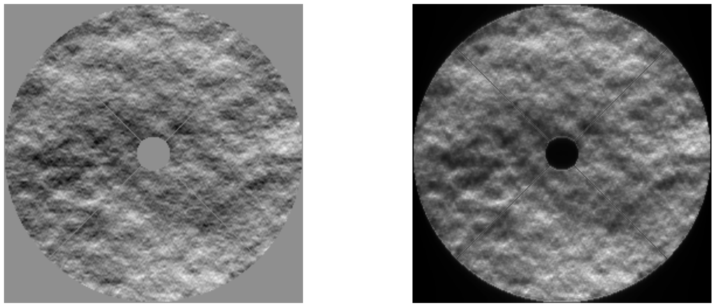

Figure 6. Simulation of AA-fluctuations (left) and corresponding Flying Shadows in the pupil plane image (right). They were obtained for a same optical turbulence at the entrance pupil and an extended source of uniform luminosity in case of total isoplanatism (see Sect.5.1). Note that we have also assumed a very large diaphragm width neglecting the diffraction filtering. As expected for the proposal system, the Flying Shadows observed in the pupil-plane in case of total isoplanatism correspond to the desired AA-fluctuations.

observation method by comparing AA-fluctuations calculated from the simulated phase $\psi_{\overrightarrow{\alpha_0}}(\overrightarrow{r})$ with the Flying Shadows expressed by the intensity variations $I(\overrightarrow{r})$.

In a first case, we consider that we have total isoplanatism i.e. $\psi_{\overrightarrow{\alpha_0}}(\overrightarrow{r})$ is the same for all $\overrightarrow{\alpha_0}$ incidence angles. We suppose also that $I_0(\overrightarrow{\alpha_0})$ is constant, which corresponds to an uniformly emitting extended-source and having an extremely large diaphragm i.e. the angular distribution $K_{\overrightarrow{\alpha_0}}(\overrightarrow{\alpha})$ is supposed to be masked only by the lower border of the diaphragm neglecting thus, the diffraction filtering. With all theses considerations, we observe that the Flying Shadows match perfectly the AA-fluctuations at the entrance pupil (see Fig. 6). Note that this result supposes also the near-field approximation hypothesis where scintillation is reasonably ignored for diurnal observations (see Sect.4.4).

As the most important condition to the validity of the method is the linearity relationship between intensity and AA-fluctuations (see Equation 1), we also confirm the linearity condition in this special case.

This result shows at the same time the accuracy of the simulation and the validity of the concept for measuring AA-fluctuations from pupil-plane images.

5.3. Solar Limb Darkening Profile's Effect

In case of solar observations with MISOLFA, the source intensity $I_0(\overrightarrow{\alpha_0})$ is not uniform but presents a strong variation from the center to the limb of the Sun.

The effect of the limb darkening profile on Flying Shadows observed in the pupil plane has been theoretically studied by Borgnino[15] in the framework of a polynomial expansion for the cases of linear and non-linear limb darkening functions.

In case of a linear darkening profile, the intensity variations are still proportional to AA-fluctuations. Contrarily, if the limb darkening profile is non-linear, the relation between intensity and AA-fluctuations is slightly non-linear. This result has also been confirmed by simulation[11] in case of total isoplanatism and near-field approximation hypothesis.

The optical effects such as anisoplanatism and limb darkening intensity variation are locally significant on a limited angular extent around diaphragm borders (see Fig. 2). We can consider in case of the Sun that the limb darkening profile is almost linear on a small angular field-of-view (few arc-seconds). We can then conclude in case of isoplanatism and the near-field approximation hypothesis that the intensity variations in pupil-plane images are proportional to the AA-fluctuations at the entrance pupil, as expressed by Equation 1.

To ensure this conclusion we use in the simulation, an approximation model for the solar limb darkening function.[16] Fig. 7 shows the linearity relationship obtained from the simulation between intensity measurements

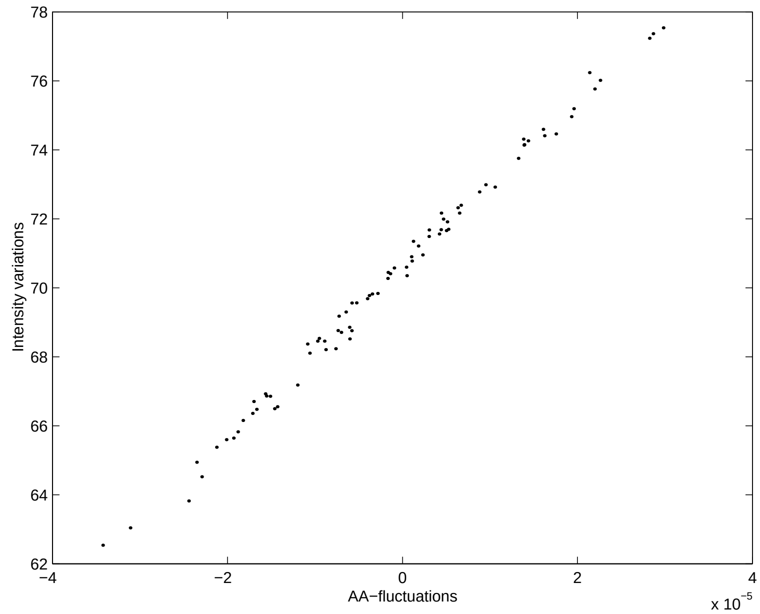

Figure 7. Good linearity observed between intensity variations in pupil-plane images (Flying Shadows patterns) and simulated AA-fluctuations at the entrance pupil (see Sect.5.1). The simulation was implemented in an isoplanatic case with $r_0 = 2cm$, $\mathcal{L}_0 = 10m$, $h = 400m$, $w_x = 5''$ and in the near-field approximation case. Both AA-fluctuations and Intensity variations are integrated over a circular photodiode area with a diameter of about $2.5cm$ on pupil entrance.

computed from the Flying Shadows in the pupil plane image and simulated AA-fluctuations at the entrance pupil.

6. DISCUSSION AND PERSPECTIVES

Anisoplanatism appears to be the most fundamental limitation in the transformation process of AA-fluctuations to intensity variations by the *pupil-plane analysis way* of MISOLFA.

We may first consider the case in which optical turbulence and hence $K_{\overrightarrow{\alpha_0}}(\overrightarrow{\alpha})$, is locally isoplanatic at least over the angular extent where the filtering by diaphragm borders occurs. In this situation, the obtained Flying Shadows correspond to the true AA-fluctuations. For large diaphragms, the intensity $I(\overrightarrow{r})$ corresponds to the sum of AA-fluctuations from isoplanatic zone with others along the diaphragm edge. This situation is the case of very low turbulent layers, a typical configuration of daytime turbulence.

In case of local anisoplanatism, we may consider $K_{\overrightarrow{\alpha_0}}(\overrightarrow{\alpha})$ varying from an angle $\overrightarrow{\alpha_0}$ to another within the extent of seeing angle believed to be diaphragm angular domain effects. The relation between intensity variations in pupil-plane images and AA-fluctuations at the entrance pupil is then questionable and could not be directly expressible. The role of the simulation is to estimate if the Flying Shadows correspond to a summation over $\overrightarrow{\alpha_0}$ of AA-fluctuations to ensure if linearity is still valid and eventually to qualify the introduced errors. It is however expected as demonstrated in Sect.4.2 that the method of observing intensity variations on the pupil-plane image remain valid for low turbulent layers.

The *pupil-plane observation way* of MISOLFA enables to measure the AA-fluctuations on the entrance pupil using intensity variations. The statistical treatment of AA-fluctuations is by far, widely investigated and implemented in nighttime site testing monitors as for the Generalized Seeing Monitor (GSM).[17] It could be then directly applied on diurnal data measurements to retrieve the statistical properties of daytime turbulence.

For example, the pupil-plane method applied to a large telescope could serve to adjust the daytime turbulence models by means of a two-dimensional covariance or structure function of AA-fluctuations.[18] These statistical functions could be obtained for every baseline and every orientation (relatively to AA-fluctuations) allowed on the pupil-plane area.

In MISOLFA, the used photodiode detectors represent various collecting surfaces of the pupil-plane. They allow fast recordings and thus an accurate intensity signal time sampling. Such measurement time series will be used to study temporal properties of the diurnal turbulence and continuously estimate the correlation time τ_0 of AA-fluctuations.

Such as for other seeing monitors like the well-known DIMM or GSM, dual measurements from photodiode pairs on the same collecting surface will allow also estimate the Fried parameter r_0. An accurate calibrating of AA-fluctuations obtained from measured intensity variations is however needed for this purpose.

The goal of using photodiode detectors with different collecting surfaces is to estimate the spatial coherence outer scale $\mathcal{L}_0$ from AA-fluctuation statistics.[19] Outer scale $\mathcal{L}_0$ has been widely investigated in case of nighttime turbulence but still unknown in case of daytime optical turbulence. However, it is expected that the values would be smaller than the ones obtained for nighttime measurements. The method used in MISOLFA will depend on the collecting surfaces of the photodiode detectors. A specific study will be developed to ensure sufficient sensitivity to outer scale effects.

Good estimation of turbulence parameters are strongly linked to AA-fluctuation measurements. Thus, we need to well understand all effects affecting the atmospheric parameter estimation from filtered AA-fluctuation measurements and how to optimize them. It will be eventually useful to include these filtering directly into models describing the filtered AA-fluctuation statistics as a function of the optical turbulence parameters.

These are all the principal short-term perspectives for this simulation.

ACKNOWLEDGMENTS

This work has been performed with support of *the Algerian Research National Program (PNR)* and the French Foreign affair Ministry in the framework of scientific cooperation between France and Algeria (contract 00 MDU 501)

REFERENCES

1. F. Laclare, C. Delmas, J. P. Coin, and A. Irbah, "Measurements and Variations of the Solar Diameter," *Solar Physics* **166**, pp. 211–229, 1996.
2. http://smsc.cnes.fr/PICARD/index.htm
3. C. Delmas, "Measurements of the Sun's Radius at Calern Observatory," *Lecture Notes in Physics* **599**, *The Sun's Surface and Subsurface : Investigating Shape and Irradiance,* Ed. : Rozelot J P, p. 196, Springer Conference Series, p. 196, 2003.
4. J. Borgnino, F. Martin, and F. Roddier, "Localisation de couches turbulentes atmosphérique par traitement optique de clichés d'ombres volantes stellaires," *Nouv. Rev. Optique* **6**, pp. 15–23, 1975.
5. J. Borgnino, and F. Martin, "Analyse statistique des déformations aléatoires d'une surface d'onde dues à la turbulence atmosphérique au voisinage du sol, I.- Exposé de la méthode, Premiers résultats," *J. Optics (Paris)* **8**, pp. 319–326, 1977.
6. J. Borgnino, and F. Martin, "Analyse statistique des déformations aléatoires d'une surface d'onde dues à la turbulence atmosphérique au voisinage du sol, II.- Estimation des fonctions de corrélation par traitement numérique," *J. Optics (Paris)* **9**, pp. 15–24, 1977.
7. J. Borgnino, and F. Martin, "Correlation between angle-of-arrival fluctuations on entrance pupil of a solar telescope," *J. Opt. Soc. Am.* **67**, pp. 1065–1072, 1977.
8. A. Irbah, J. Borgnino, F. Laclare, and G. Merlin, "Isoplanatism and high spatial resolution solar imaging," *Astron. Astrophys.* **276**, pp. 663–672, 1993.
9. A. Irbah, M. Chibani, L. Lakhal, A. Berdja, J. Borgnino, F. Martin, and P. Assus, "MISOLFA : a generalized solar seeing monitor," *SF2A-2001: Semaine de l'Astrophysique Française,* Eds.: F. Combes, D. Barret, F. Thévenin, p.59, published by EdP-Sciences, Conference Series, meeting held in Lyon, France, May 28-June 1st, 2001.

10. A. Berdja, A. Irbah, and J. Borgnino, "Simluation of the anisoplanatic angle-of-arrival fluctuations measured on the solar edge images," *SF2A-2002: Semaine de l'Astrophysique Française*, Eds.: F. Combes and D. Barret, p. 215, EdP-Sciences (Editions de Physique), Conference Series, meeting held in Paris, France, June 24-29, 2002.
11. A. Berdja, A. Irbah, J. Borgnino, and F. Martin, "Simulation of Angle-of-Arrival fluctuations as observed in the MISOLFA pupil-plane," *SF2A-2003: Semaine de l'Astrophysique Française*, Eds.: F. Combes, D. Barret and T. Contini, p. 158, EdP-Sciences, Conference Series, meeting held in Bordeaux, France, June 16-20, 2003.
12. A. Bouzid, A. Irbah, J. Borgnino, and H. Lanteri, "Atmospheric Turbulence Profile Estimation from Fluctuation Analysis of Extended Object Images," *European Rocket and Balloon Programs and Related Research, Proceedings of the* 14^{th} *ESA Symposium*, Edited by B. Schürmann. European Space Agency, ESA-SP, **Vol. 437**, p.453, 1999.
13. J. Borgnino, and J. Vernin, "Experimental verification of the inertial model of atmospheric turbulence from solar limb motion," *J. Opt. Soc. Am.* **68**, pp. 1056–1062, 1978.
14. T. Nakajima, "Signal-to-noise ratio of the bispectral analysis of speckle interferometry," *J. Opt. Soc. Am.* **5**, pp. 1477–1491, 1988.
15. J. Borgnino, "Étude de la dégradation des images astronomiques diurnes par analyse statistique des fluctuations d'angle d'arrivée," Doctorat thesis, Nice university, 1978.
16. L. Lakhal, A. Irbah, C. Aime, J. Borgnino, and F. Martin, "Estimation of turbulence parameters from solar observations," *Proc. SPIE, Optics in Atmospheric Propagation and Adaptive Systems IV*, **Vol. 4538**, p. 112-118, 2002.
17. A. Ziad, R. Conan, A. ToKbvinin, F. Martin, and J. Borgnino "From the Grating Scale Monitor to the Generalized Seeing Monitor," *Applied Optics* **39**, p. 30, 2000.
18. R. Avila, A. Ziad, J. Borgnino, F. Martin, A. Agabi and A. A. Tokovinin, "Theoretical spatio-temporal analysis of angle of arrival induced by atmospheric turbulence as observed with the Grating Scale Monitor Experiment," *J. Opt. Soc. Amer. A* **14**, p. 11, 1997.
19. A. Ziad, J. Borgnino, F. Martin, and A. Agabi, "Experimental estimation of the spatial-coherence outer scale from a wavefront statistical analysis," *Astronomy and Astrophysics* **282**, pp. 1021–1033, 1994.